Open Access

Influences of Assault Blocks on Rotor Vibrations in AMB System

Zhu Yili[*] and Zhang Yongchun

Department of Electrical Engineering, Changzhou Institute of Technology, Changzhou, Jiangsu, 213002, P.R. China

Abstract: In an active magnetic bearing (AMB) system, the rotor always rotates at extremely high speed which always accompany with huge vibrations and noises. Most of the former researches associated with reducing the rotor vibrations are mainly focused on the control methods of AMB. A new method of installing series of assault blocks in the rotor is proposed to reduce the rotor vibrations. Firstly, the dynamic models of rotor supported by AMB considering the influences of assault blocks are established. Then, both dynamic simulations with and without assault blocks are carried out separately using the real-time AMB support dynamic stiffness. The rotor vibration displacements are mainly analyzed. Finally, relevant experiments are made to verify the theoretical results. Both theoretical and experimental results validated the advantages of using assault blocks.

Keywords: Active magnetic bearing, assault block, dynamic stiffness, rotor vibration.

1. INTRODUCTION

AMB have many advantages over conventional mechanical bearings, such as active control, no mechanical contact, no friction, no lubrication and high speed. The rotor in AMB system always rotates at extremely high speed to improve its working performances. Because of the rotor unbalance, the rotor will has certain vibration synchronous with rotor frequency. Most of the former researchers tried to modify the control system to reduce the unbalance displacement vibrations.

Jing, *et al.* injected an additional force to AMB system to restrict the unbalance force [1]. Reference [2] proposed an adaptive auto-centering approach, which can realize on-line identification of rotor unbalance and force compensation. Taguchi, *et al* proposed a vibration control system to deal a sudden sinusoidal disturbance [3]. Mizuno, *et al.*, proposed pole-zero cancellation compensation to realize displacement, current and force regulations [4]. A LQR scheme for vibration control in AMB system to reduce the unbalance vibrations is proposed by Arias, *et al.* [5]. Moreover, iterative learning control is applied in the unbalance compensation for AMB system [6-10]. However, most of the existing methods to reduce the rotor unbalance vibrations in AMB system are based on the control system, which may to some extent influence the AMB system stability

In this paper, a series of assault blocks are added to the rotor system. Both AMB mathematical model and rotor dynamic model are established. And based on hertz contact theory, the contact model between assault block and rotor is established. Then influences of those installed assault blocks

on the rotor vibrations are theoretically and experimentally analyzed.

2. AMB STIFFNESS ANALYSIS

Accurate AMB support stiffness is necessary to obtain accurate rotor vibration characteristics. Fig. (**1**) presents the AMB system control diagram.

In the control diagram, i_{cx1} is the control current; v_s is displacement sensor output; v_r is input of PID controller, which is linear with rotor vibration displacement x_1; x_0 is the balanced air gap, here x_0 = 1.25e-4 m; $G_{A,S}$ are the linear amplifier power gain and sensor gain respectively, here G_A = 0.4 A/V and G_S = 20000 V/m. According to the control diagram, the relationship between control current and rotor vibration displacement can be expressed as:

$$i_{cx1} = v_r \cdot G_{PID} \cdot G_A = (2.5 - v_s) \cdot G_{PID} \cdot G_A$$
$$= [2.5 - (0.5x_0 + x_1) \cdot G_S] \cdot G_{PID} \cdot G_A \qquad (1)$$
$$= -8000 \cdot x_1 \cdot G_{PID}$$

The resultant force acting on the rotor in one direction can be linearized as

$$F_{x1} = K_{xx1} \cdot x_1 + K_{ix1} \cdot i_{cx1} \qquad (2)$$

Where $K_{xx1} = \mu_0 A N^2 I_0^2 / x_0^3$ is the displacement stiffness, and $K_{ix1} = \mu_0 A N^2 I_0 / x_0^2$ is the current stiffness, they can be calculated using the parameters listed in Table **1**. As the complete structure symmetric of the radial magnetic bearings, the displacement stiffness and current stiffness of each degree are equal.

Substituting formula (1), the formula (2) becomes

*Address correspondence to this author at the Department of Electrical Engineering, Changzhou Institute of Technology, Changzhou, Jiangsu, 213002, P.R. China; Tel: +86 0519 85217620; E-mail: nuaazyl@163.com
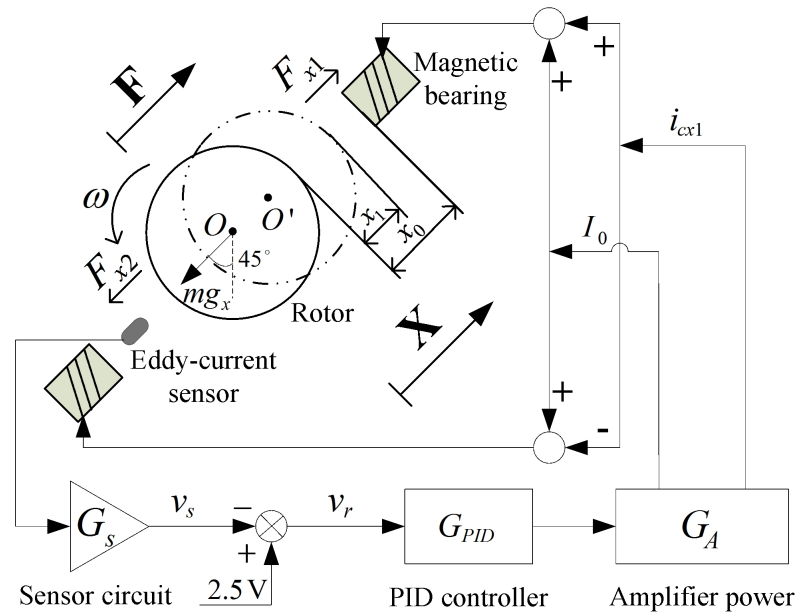
Fig. (1). One-degree of freedom (DOF) AMB system control diagram.

Table 1. Parameters of AMB.

Parameter	Value
Pole area A (m^2)	1.96e-4
Bias current I_0 (A)	2
Numbers of the coils N	130
Differential coefficient k_d	1.4e-3
Integral coefficient k_i	10
Proportional coefficient k_p	2.3
Gap of the rotor at balance position x_0 (mm)	0.25
Filtering time constant τ_d	7e-5
Air permeability μ_0 (V·s/(A·m))	4πe-7

$$F_{x1}(j\omega) = -j8000K_{ix1}I_m\left[G_{PID}(j\omega)\right]x_1(j\omega)$$
$$+ K_{x1}x_1(j\omega) - 8000K_{ix1}R_e\left[G_{PID}(j\omega)\right]x_1(j\omega) \quad (3)$$

Where ω is the rotor rotational velocity.

The transfer function of PID controller is

$$G_{PID}(s) = k_p + \frac{k_i}{s} + \frac{k_d s}{1+\tau_d s} \quad (4)$$

The parameters in the formula are listed in Table **1**.

The stiffness and damping of AMB can be deduced from formula (3):

$$\begin{cases} K = -8000K_{ix1}R_e\left[G_{PID}(j\omega)\right] + K_{xx1} \\ C = \dfrac{-8000K_{ix1}I_m\left[G_{PID}(j\omega)\right]}{\omega} \end{cases} \quad (5)$$

The parameters in the formula are listed in Table **1**.

Then the AMB dynamic stiffness can be written as [10].

$$K_d = \sqrt{K^2 + (C\omega)^2} \quad (6)$$

Using the parameters of AMB presented in Table **1**, the AMB dynamic stiffness can be obtained.
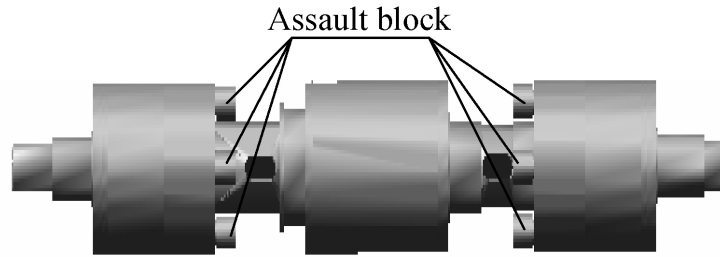
Fig. (2). Proposed rotor three-dimensional model.
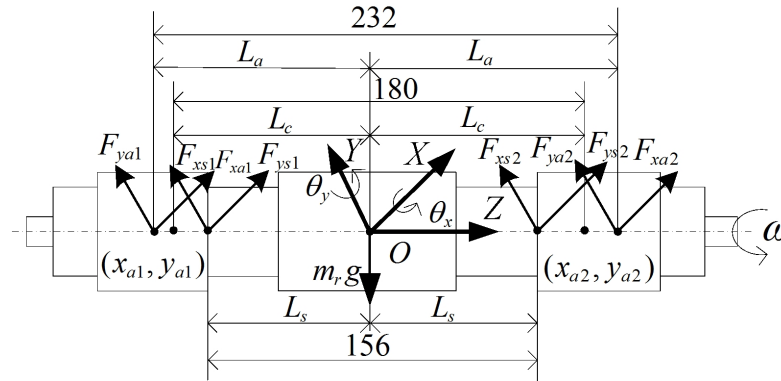
Fig. (3). Rotor structure and load-carrying model.

3. DYNAMIC MODELS

3.1. Rotor Model

Fig. (**2**) gives the rotor three-dimensional model with assault blocks. Those assault blocks are located in the outside of the rotor for clear statement. In practice, the eight assault blocks are installed in the relevant holes of the rotor.

As the AMB thrust force is in the rotor axial direction, and the rotor does not exist unbalance in axial direction, the axial subsystem can be separated from the other four radial DOFs. Fig. (**3**) gives the rotor force analysis in the four radial directions, and the dimensions are in millimeters. Where O is the rotor mass center; L_a and L_c are the distances between radial magnetic bearing and rotor barycenter, radial displacement sensor and rotor barycenter respectively; θ_x and θ_y are the rotor rotational displacement around axis X and axis Y respectively. Each magnetic force is defined as F_n ($n = xaj$ or yaj, $j = 1$, 2 denote left and right side, respectively); each counterforce from one hand assault blocks is defined as F_m ($m = xsj$ or ysj). The magnetic force can be calculated using equation 6. While, detailed collision model between rotor and assault blocks should be established to calculate each counterforce.

Rigid rotor model is established to analyze the dynamic responses. According to Fig. (**3**), the motion formula can be expressed as:

$$M\ddot{X}_o + G\dot{X}_o = AF_a + SF_s - F_c \qquad (7)$$

Where M is the rotor mass matrix, X_o is the displacement vector of rotor barycenter, G is the rotor gyro torque matrix, A and S are the introduced parameter matrix, F_a, F_S, F_c are electromagnetic force, assault block counterforce and centrifugal force matrix respectively.

$$M = diag\left(m_r, m_r, J, J\right) \qquad (8)$$

Where m_r is the rotor mass; and J is rotor transverse moment of inertia (MOI).

$$X_o = \begin{bmatrix} x_o & y_o & \theta_x & \theta_y \end{bmatrix}^T \qquad (9)$$

Where x_o and y_o are the rotor barycenter displacements in X and Y direction respectively.

$$G = \begin{bmatrix} 0 & 0 & 0 & 0 \\ 0 & 0 & 0 & 0 \\ 0 & 0 & 0 & \omega J_z \\ 0 & 0 & -\omega J_z & 0 \end{bmatrix} \qquad (10)$$

Where J_z is the rotor polar MOI;

$$A = \begin{bmatrix} 1 & 0 & 1 & 0 \\ 0 & 1 & 0 & 1 \\ 0 & L_a & 0 & -L_a \\ -L_a & 0 & L_a & 0 \end{bmatrix} \qquad (11)$$
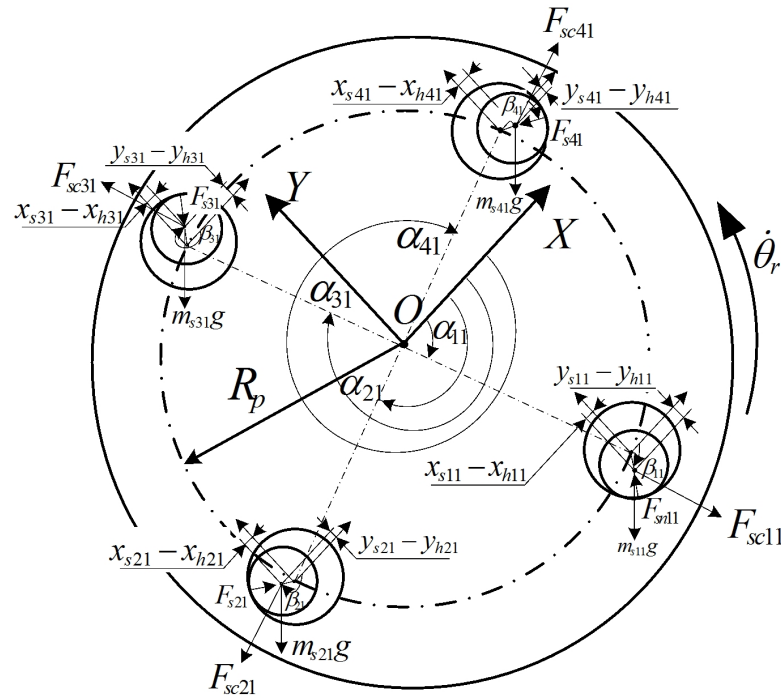
Fig. (4). Contact model between assault blocks and rotor.

$$S = \begin{bmatrix} 1 & 0 & 1 & 0 \\ 0 & 1 & 0 & 1 \\ 0 & L_s & 0 & -L_s \\ -L_s & 0 & L_s & 0 \end{bmatrix} \qquad (12)$$

$$F_a = \begin{bmatrix} F_{xa1} & F_{ya1} & F_{xa2} & F_{ya2} \end{bmatrix}^T \qquad (13)$$

$$F_s = \begin{bmatrix} F_{xs1} & F_{ys1} & F_{xs2} & F_{ys2} \end{bmatrix}^T \qquad (14)$$

$$F_c = \begin{bmatrix} m_r e_r \omega^2 \cos(\omega t) + m_r g_x \\ m_r e_r \omega^2 \sin(\omega t) + m_r g_y \\ 0 \\ 0 \end{bmatrix} \qquad (15)$$

Where e_r is the rotor unbalance, g_x and g_y are the gravity acceleration in X and Y directions.

The real time support force of magnetic bearings can be calculated using the dynamic stiffness and displacement detected by the relevant displacement sensor. So the displacement vector X_o of the rotor barycenter should be converted to the rotor displacement vector X_c at position of the radial displacement sensors.

$$X_o = D_1 X_c \qquad (16)$$

Where $X_c = \begin{bmatrix} x_{c1} & y_{c1} & x_{c2} & y_{c2} \end{bmatrix}^T$ and

$$D_1 = \frac{1}{2L_c} \begin{bmatrix} L_c & 0 & L_c & 0 \\ 0 & L_c & 0 & L_c \\ 0 & 1 & 0 & -1 \\ -1 & 0 & 1 & 0 \end{bmatrix} \qquad (17)$$

In the same way, the displacement vector X_s at the two ends of assault blocks can be derived as

$$X_s = D_2^{-1} D_1 X_c \qquad (18)$$

Where $X_s = \begin{bmatrix} x_{s1} & y_{s1} & x_{s2} & y_{s2} \end{bmatrix}^T$ and

$$D_2 = \frac{1}{2L_s} \begin{bmatrix} L_s & 0 & L_s & 0 \\ 0 & L_s & 0 & L_s \\ 0 & 1 & 0 & -1 \\ -1 & 0 & 1 & 0 \end{bmatrix} \qquad (19)$$

Then the rotor motion equation (7) can be rewritten as

$$MD_1 \ddot{X}_c + GD_1 \dot{X}_c = AF_a + SF_s - F_c \qquad (20)$$

3.2. Contact Model

Taking the left end for example, the contact model between assault block and rotor is established, as shown in Fig. (**4**). During normal operation, the collisions between assault blocks and rotor play the role of reducing vibrations. There are four assault blocks at one end, the position angles are α_{11}、 α_{21}、 α_{31} and α_{41}, respectively. The contact angles

Table 2. Specification of simulation parameters.

Parameter	Value
Rotor imbalance eccentricity e_r (mm)	0.008
Gravity acceleration in X and Y direction respectively g_x, g_y (m/s^2)	6.93
Rotor polar MOI J_z (kg.mm^2)	3.8E+2
Rotor transverse MOI J (kg.mm^2)	1.612E+4
Rotor mass m_r (kg)	2.14
Journal radius R_r (mm)	5.875
Assault block mass m_s (g)	2.5
Assault block radius R_s (mm)	9
Assault hole radius R_h (mm)	10

between each impact normal direction and X axes are β_{11}, β_{21}, β_{31} and β_{41}, respectively. The coordinate position of the assault block center is $(x_{s\varsigma 1}, y_{s\varsigma 1})$, where $\varsigma = 1,2,3,4$. And the relevant coordinate position of the assault hole center in the rotor is $(x_{h\varsigma 1}, y_{h\varsigma 1})$, where $\varsigma = 1,2,3,4$.

Based on the hertz contact theory [10], the impact force between the ς th assault block and hole can be written as follows:

$$F_{s\varsigma 1} = \begin{cases} K_s \delta_{s\varsigma 1}^{10/9} \left(1 + 0.12 \dot{\delta}_{s\varsigma 1}\right), & \delta_{s\varsigma 1} > 0 \\ 0, & \delta_{s\varsigma 1} \leq 0 \end{cases} \quad (21)$$

Where the contact stiffness K_s depends on material property and contact geometry: here $K_s = 2.4E+9$ N/m; the penetration depth $\delta_{s\varsigma 1} = r_{s\varsigma 1} - (R_h - R_s)$, where R_h and R_s are the radiuses of assault hole and assault block respectively, and $r_{s\varsigma 1} = \sqrt{(x_{s\varsigma 1} - x_{h\varsigma 1})^2 + (y_{s\varsigma 1} - y_{h\varsigma 1})^2}$.

According to the geometrical relationship, the impact force can be decomposed into two component forces in X and Y directions.

$$\begin{cases} F_{xs\varsigma 1} = -F_{s\varsigma 1} \dfrac{x_{s\varsigma 1} - x_{h\varsigma 1}}{r_{\varsigma 1}} \\ F_{ys\varsigma 1} = -F_{s\varsigma 1} \dfrac{y_{s\varsigma 1} - y_{h\varsigma 1}}{r_{\varsigma 1}} \end{cases} \quad (22)$$

Then the motion equation of the ς th assault block can be expressed as

$$\begin{bmatrix} m_s & 0 \\ 0 & m_s \end{bmatrix} \begin{bmatrix} \ddot{x}_{s\varsigma 1} \\ \ddot{y}_{s\varsigma 1} \end{bmatrix} = \begin{bmatrix} F_{xs\varsigma 1} \\ F_{ys\varsigma 1} \end{bmatrix} \quad (23)$$

In the same way, the impact forces and motion equations of the other assault blocks can be obtained. Considering all the impact forces, the assault block counterforce vector can be rewritten as

$$F_s = \left[\sum_{\varsigma=1}^{4} F_{xs\varsigma 1} \quad \sum_{\varsigma=1}^{4} F_{ys\varsigma 1} \quad \sum_{\varsigma=1}^{4} F_{xs\varsigma 2} \quad \sum_{\varsigma=1}^{4} F_{ys\varsigma 2} \right]^T \quad (24)$$

4. SIMULATION RESULTS

Using a variable time-step fourth order Runge-Kutta [12] integration algorithm, both of the numerical solutions using assault blocks and without assault blocks are respectively obtained. The detailed parameters are listed in Table **2**.

Fig. (**5a**)-(**b**) show simulation displacements of the left journal from 0 to 0.1 second after AMB works, and the rotor rotating speed is 12 000 r/min. The following conclusions can be obtained: (1) because of the rotor gravity, the vibration center does not locate at the established origin of coordinates; (2) the use of assault blocks can effectively reduce the rotor vibration displacements, and the vibration amplitude has been reduced by about 35%; (3) compared with the rotor without assault blocks, the vibration amplitudes of the rotor installed assault blocks are not equal for the series of internal collisions.

5. EXPERIMENT RESULTS

Fig. (**6**) shows the experimental facilities necessary for measurement. Three boards NI-9215 from National Instruments are chosen to collect the rotor displacement signals, and the relevant collection software is established on the platform of LABVIEW. Those collected signals are saved in computer for further analysis.

Fig. (**7**) shows the output waveforms of left radial sensor in X direction with and without assault blocks at the rotor rotational speed 12 000 r/min. The displacement sensor sensitivity is 20 mv/μm. It can be seen that the rotor radial displacements with assault blocks are obviously smaller, and
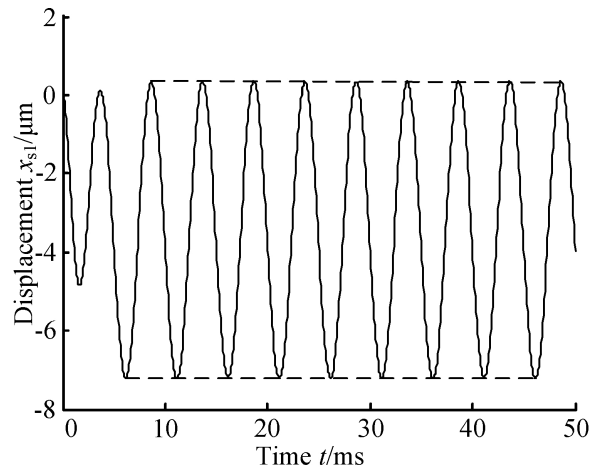
(**a**) Rotor without Assault Blocks.
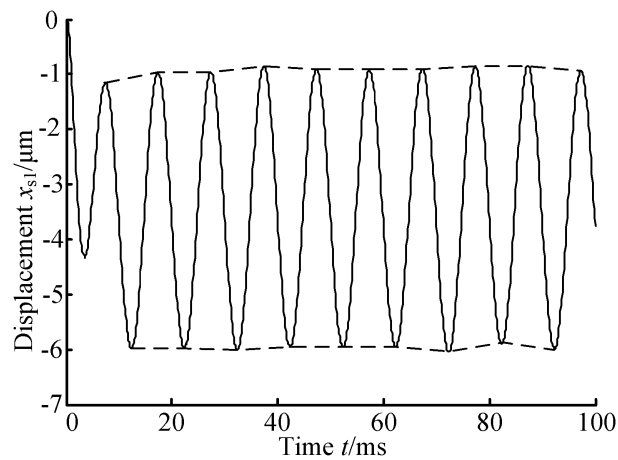
(**b**) Rotor Installed Assault Blocks.

Fig. (5). The left rotor center displacement in *X* direction.
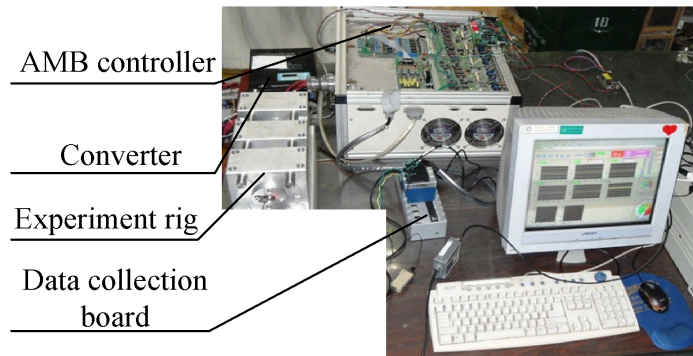
Fig. (6). Photograph of the experimental facilities.

the peak to peak amplitude has been reduced about 30%. Also, the rotor vibration amplitudes with assault blocks are not equal.

CONCLUSION

(1) The rotor vibration displacements are achieved through solving those established mathematical models. And the model accuracy is verified by the following experiments.

(2) Assault blocks are proposed to be installed in the rotor system to reduce the rotor vibrations. Both simulation results and experiment results prove their effects. And the peak to peak amplitude has been reduced by about 30%~35%.

As a result, except for the methods of modifying AMB controller system, the rotor vibrations can also be reduced by installing proper assault blocks in the rotor.
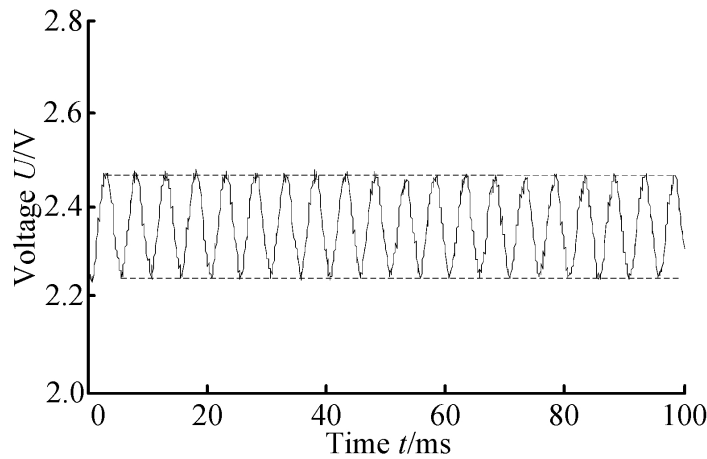
(**a**) Rotor without Assault Blocks.
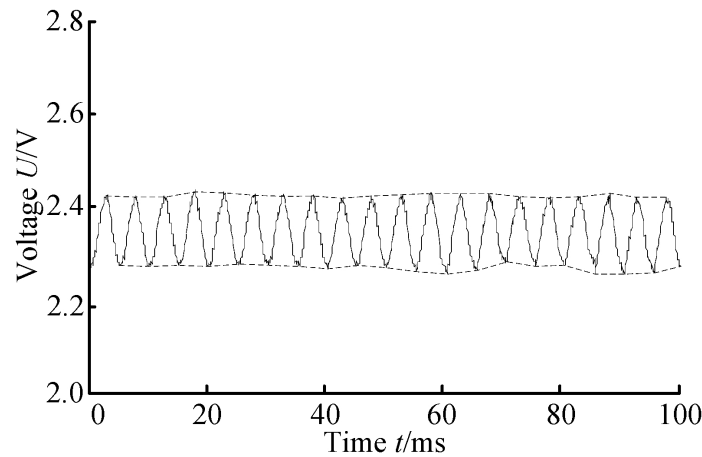
(**b**) Rotor Installed Assault Blocks.

Fig. (7). The outputs of displacement sensor obtained by experiments.

CONFLICT OF INTEREST

The authors confirm that this article content has no conflict of interest.

ACKNOWLEDGEMENTS

REFERENCES

[1]   L. Yu, The system of rotor of controllable magnetic bearings, Xi'an, 2003, pp.100-125.

[2]   M. Q. J. Minqing, Z. X. Li, and M. Luo, "Unbalance response and touch-rubbing threshold speed of rotor subjected to nonlinear magnetic forces", *Chinese Journal of Mechanical Engineering*, vol. 21, no. 2, pp. 1-4, 2008.

[3]   K. Y. Lum, V. T. Coppola, and D. S. Bernstein, "Adaptive autocentering control for an active magnetic bearing supporting a rotor with unknown mass imbalance", *IEEE Transactions on Control Systems Technology*, vol. 4, no. 5, pp. 587-597, 1996.

[4]   N. Taguchi, T. Ishimatsu, and S. J. Woo, "Unbalance compensation of magnetic bearings", In: *Proceedings 20th International Conference on Industrial Electronics, Control and Instrumentation, Industrial*, Bologna, Italy, 1994, pp. 2051-2056.

[5]   T. Mizuno, "An unified approach to controls for unbalanced compensation in active magnetic bearings", In: *Proceedings of IEEE International Conference on Control Applications*, Trieste, Italy, 1998, pp. 1063-1067.

[6]   M. M. Arias, and N. G. Silva, "Finite element modeling and unbalance compensation for a two disks asymmetrical rotor system", In: *Proceedings of 5th International Conference on Electrical Engineering, Computing Science and Automatic Control*, Mexico City, Mexico, 2008, pp. 386-391.

[7]   B. T. Costic, M. S. Queiroz, D. N. Dawson, "A new learning control approach to the active magnetic bearing benchmark system", In: *Proceedings of 2000 American Control Conference*, Chicago, IL, USA, 2000, pp. 2639-2643.

[8]   H. G. Chiarini, and P. S. Mandolesi, "Unbalance compensation for active magnetic bearings using ILC", In: *Proceedings of the 2001 IEEE International Conference on Control Applications*, Mexico City, Mexico, 2001, pp. 58-63.

[9]   B. Chao, D. Z. Wu, and Q. Jing, "Automatic learning control for unbalance compensation in active magnetic bearings", *IEEE Transactions on Magnetics*, vol. 41, no. 7, pp. 270-280, 2005.

[10]   Y. H Sun, Y. S. Ho, and L. Yu, "Dynamic stiffnesses of active magnetic thrust bearing including eddy-current effects", *IEEE Transactions on Magnetics,* vol. 45, no. 1, pp. 139-149, 2009.

[11]   H. Hertz, "On the contact of elastic solids", *Journal Für Die Reine und Angewandte Mathematik*, vol. 92, pp. 20-35, 1881.

[12]   E. Hairer, S.P. Norsett, and G. Wanner, *Solving ordinary differential equations I: Nonstiff Problem*. Springer, New York, 1993, pp. 27-59.